Magyarhoni Földtani Társulat
Földtani Közlöny
Hungarian Geological Society

156/3, 257–275., Budapest, 2026

DOI: 10.23928/foldt.kozl.2026.156.3.257

Intracellular bodies in magnetotactic bacteria and their possible geochemical significance

KÖVÉR, Regina[1,2], PEKKER, Péter[1,2], RÁCZ, Kornél[1,2], PÓSFAI, Mihály[1,2]

[1]Research Institute of Biomolecular and Chemical Engineering, University of Pannonia, Veszprém, Hungary
[2]HUN-REN–PE Environmental Mineralogy Research Group, Veszprém, Hungary

kover.regina@mk.uni-pannon.hu
pekker.peter@mk.uni-pannon.hu
racz.kornel@mk.uni-pannon.hu
posfai.mihaly@mk.uni-pannon.hu

Mágneses baktériumok sejten belüli zárványai és lehetséges geokémiai szerepük

Összefoglalás

A mágneses baktériumok (MB) a bennük található, membránnal körülvett, láncba rendeződő vas-oxid/vas-szulfid ásványok (magnetoszóma) által képesek érzékelni a Föld mágneses erővonalait, és ezek mentén mozogva találják meg a számukra legkedvezőbb oxigénszintet a vízben. Habár legfőbb jellegzetességük, hogy mágneses nanokristályokkal rendelkeznek, ezeken kívül tartalmazhatnak polifoszfát (poliP), elemi kén (S) és amorf kalcium-karbonát (ACC) zárványokat is. A Nagyvázsonyhoz közeli Kinizsi-forrásból különböző évszakokban (ősszel, télen és tavasszal) gyűjtött, MB-tartalmú mintákat transzmissziós elektronmikroszkóppal (TEM) vizsgáltuk. Egyrészt a minták friss állapotait, másrészt – azokat laboratóriumban tárolva – az idő múlásával bekövetkező változásait figyeltük. A friss minták esetén elsődleges célunk az volt, hogy egy előzetes képet kapjunk a mintákban található sejttípusokról és ezek zárványairól. Megfigyelhető, hogy egy adott sejtben lévő zárvány típusa összefügg a sejt egyéb jellemzőivel, de a zárványok jelenléte évszaktól függ. Következésképpen a zárvány típusa genetikailag kontrollált, de ezzel egyidejűleg a környezet által is befolyásolt. Mivel a MB sejtek folyamatosan le-föl mozognak a mikrooxikus és anoxikus zóna között, poliP és S zárványaik révén fontos szerepet játszhatnak a foszfor és a kén geokémiai eloszlásának kialakításában, illetve a tápanyagciklusban. A laboratóriumban tárolt mintákban néhány hónap elteltével más-más MB sejttípusok dominanciája volt megfigyelhető. Az évszakonként tapasztalt változások mintázatainak elemzéséhez a téli mintát négy egyenlő részre osztva, három hónapon át havi rendszerességgel vizsgáltuk. Az idő múlásával az egyes mikrokozmoszokban változott a domináns sejttípus, és általában a poliP-tartalmú sejttípusok váltak uralkodóvá a mintákban. Három coccus sejtről elektrontomográfiás felvétel készült, mely révén a sejten belüli zárványok egymáshoz viszonyított elhelyezkedése is vizsgálhatóvá vált. A zárványok elrendeződése a sejt egyenletes tömegeloszlásának megfelelő, és segíti a sejt úszását a mágnesség által meghatározott irányban. Bizonyos coccus sejttípusok a sejt méretéhez viszonyítva rendkívül nagy poliP-zárványokat tartalmaztak. Megfigyeléseink felvetik a MB sejtek technológiai alkalmazásának lehetőségét a foszfor oldatból való eltávolítására.

Tárgyszavak: mágneses baktérium, magnetit, polifoszfát, elemi kén, amorf kalcium-karbonát, transzmissziós elektronmikroszkópia (TEM)

Summary

Magnetotactic bacteria (MTB) are able to sense the Earth's magnetic field direction through chains of membrane-bound iron oxide or iron sulfide minerals, known as magnetosomes. By aligning and migrating along these magnetic field lines, the cells are able to locate their position within optimal oxygen gradients in aquatic environments. Although the presence of magnetic nanocrystals is their most distinctive characteristic, MTB may also contain intracellular granules of polyphosphate (polyP), elemental sulfur (S), and amorphous calcium carbonate (ACC). MTB-containing samples collected from Kinizsi-spring, near Nagyvázsony in autumn, winter and spring were studied using transmission electron microscopy. We investigated both the freshly collected samples and the changes that occurred over time during laboratory storage. Regarding the fresh samples, our primary aim was to obtain a preliminary overview of the cell types and their intracellular inclusions. It was observed that the type of inclusion – present within a given cell type – was associated with other cellular characteristics, whereas the occurrence of inclusions varied with season. These findings suggest that inclusion type is under genetic control but is simultaneously influenced by environmental conditions. As magnetotactic bacteria (MTB) continuously migrate between microoxic and anoxic zones, their polyphosphate (polyP) and elemental sulfur (S) inclusions may play an important role in the biogeochemical cycling of phosphorus and sulfur, and in shaping their

distribution within aquatic environments. In the laboratory-stored samples, shifts in the dominance of different MTB cell types were observed after several months. To analyze temporal patterns in greater detail, the winter sample was divided into four equal subsamples and examined monthly over a three-month period. Over time, the dominant cell type changed within each microcosm and polyphosphate (polyP)-containing cell types generally became predominant. Electron tomography was performed on three coccoid cells, enabling the three-dimensional assessment of the spatial arrangement of intracellular inclusions. The distribution of inclusions was consistent with a balanced mass distribution within the cell and may facilitate swimming along magnetically guided trajectories. Some coccoid cell types contained extremely large polyP inclusions relative to their cell size. These observations highlight the potential of MTB for technological applications, particularly in the removal of phosphorus from aqueous solutions.

Keywords: magnetotactic bacteria, magnetite, polyphosphate, elemental sulfur, amorphous calcium carbonate, transmission electron microscopy (TEM)

Introduction

Since their discovery in 1975 (BLAKEMORE 1975), several scientific fields have regarded magnetotactic bacteria (MTB) as a curiosity. Study of MTB comprises an interdisciplinary research topic, since the bacteria and their inclusions are of interest from biological, physical, crystallographical and earth sciences perspectives. MTB are aquatic, flagellated microorganisms. They behave as living compasses, since each cell is aligned by the local geomagnetic field. The cells then have to swim along the geomagnetic field lines, thereby efficiently finding their preferred habitat in environments characterized by vertical concentration gradients (FRANKEL et al. 1997). The magnetically guided movement of MTB is called magnetotaxis.

The magnetic behavior of MTB cells arises from the presence of intracellular, magnetic iron oxide (magnetite) (FRANKEL et al. 1979) or iron sulfide (greigite) particles (MANN et al. 1990, PÓSFAI et al. 1998), which are enclosed in a phospholipid bilayer membrane (BAZYLINSKI & FRANKEL 2004, PÓSFAI et al. 2013). The iron-rich particle and its membrane together are called a magnetosome. Magnetosomes typically form chains (that can be single, double or multiple) but the cells of some other MTB taxa contain partially scattered magnetosomes (PÓSFAI et al. 2013).

Even though the special properties of intracellular magnetic nanocrystals – strain-specific morphologies, typically defect-free structures and chemical purity – were the subject of intense scientific interest (BAZYLINSKI & FRANKEL 2004, FAIVRE & SCHÜLER 2008), questions still remain, particularly about the growth and evolutionary utility of magnetite particles with non-equilibrium shapes. For magnetite, the {111} octahedron is the equilibrium form (under most conditions). However, in MTB cubooctahedral, elongated "prism" and bullet-shaped magnetite morphologies have been distinguished (DEVOUARD et al. 1998, LEFÈVRE et al. 2011, PÓSFAI et al. 2013, LI et al. 2020). In the present study we discuss only briefly the properties of magnetic nanocrystals in MTB and use the characteristic shapes and chain structures of magnetite magnetosomes for the distinction of specific bacterial strains.

In addition to magnetite crystals, other types of intracellular inclusions also occur in MTB cells, due to the fact that several biomineralization processes may occur simultaneously within them. Because of their inclusions, MTB may play important roles in biogeochemical cycles (GOSWAMI et al. 2022), since they can enrich either nutrients or geochemically significant elements. The focus of the present study is on phosphorus-, sulphur- and calcium-bearing intracellular inclusions that have been mentioned mostly in passing in the MTB literature.

Polyphosphate (polyP) inclusions are found in the cells of all living organisms (HUPFER et al. 2007). Polyphosphate is an amorphous polymer that links varying numbers of orthophosphate units via phosphoanhydride bonds, resulting in polyP particles of varying sizes. PolyP granules of MTB are not surrounded by a membrane (KEIM et al. 2005). PolyP has a multi-facetted role in cell function: participates in phosphorus storage, energy balance, and ATP, RNA and DNA production (DIAZ et al. 2008, POWELL et al. 2009, DAHL et al. 2018, CHRIST et al. 2020, DENONCOURT & DOWNEY 2021). The storage of P is essential for bacterial cells for their long-term survival (KIM et al. 2002, MASON-JONES et al. 2022). Some MTB that belong to the Magnetococcaceae family are known to produce huge polyP inclusions (RIVAS-LAMELO et al. 2017), and were implicated in the P cycle in Lake Pavin (France), a stratified, deep-water body. In a special marine environment, the Black Sea, magnetotactic cocci were shown to play a major role in the transport of phosphorus across the oxic-anoxic transition zone (SCHULZ-VOGT et al. 2019).

Elemental sulfur (S) was also found in MTB cells, though much less frequently than polyP. The presence of S inclusions was attributed to the oxidation of hydrogen sulfide or thiosulfate (KEIM et al. 2005). The S inclusions were shown to be enclosed by either a protein shell or a lipid bilayer membrane, providing structural boundary from the surrounding cytosolic environment (FULLER 1999, KEIM et al. 2005). According to KEIM et al. (2005), S inclusions do not have a specific number or fixed location within the cells in the studied marine samples, and may play a role in cellular energy and nutrient storage mechanisms. The presence of S inclusions in MTB might also have some geochemical significance. Elemental S was recently found to have a profound impact on the formation of vast amounts of pyrite at the ocean floor, as S is converted into pyrite by sulfur-reducing bacteria (SEKERCI et al. 2025).

The discovery of intracellular amorphous calcium carbonate (ACC) particles in cyanobacteria was an unexpected

finding (Couradeau et al. 2012) that challenged some long established geochemical paradigms about microbial calcification (Benzerara et al. 2014). In the last ten years, various microorganisms were found to contain intracellular ACC (Mangin et al. 2025), among them MTB as well (Rivas-Lamelo et al. 2017). ACC particles are located inside membrane-bound vesicles, and their formation and the maintenance of their stability require energy investment. It is likely that ACC inclusions play a role in regulating cell movement and may also function as ballast materials (Monteil et al. 2021). The formation of ACC is not regulated by a single gene; rather, given its evolutionary background, it may have evolved along several different lineages (Mangin et al. 2025).

Our present study was motivated by the discovery of a large number of various intracellular inclusions in strains of MTB collected from the sediment of a pond (Kinizsi-spring, Nagyvázsony, Hungary). Our original goal was to collect MTB in order to analyze the shapes of their magnetite magnetosomes using transmission electron microscopy (TEM). However, in the TEM micrographs the wealth and variability of intracellular inclusions other than magnetite were striking, prompting us to dedicate a separate study to this topic. Below we describe polyP, S and ACC inclusions in various types of MTB cells and present some data on the changes in the type and amount of inclusions over time. While we have no information on the specific biomineralization processes that led to the formation of intracellular inclusions and can only speculate on their geochemical consequences, our study intends to serve as a baseline for further studies.

Samples and methods

Magnetotactic bacteria (MTB) were collected from a pond that collects the water of Kinizsi-spring. This karstic spring is located near Nagyvázsony, in the Balaton Uplands, Hungary, in a forest, on a favored hiking trail (*Fig. 1A*). The spring is located at 46.979507, 17.660083, draining the Nagyvázsony Limestone Formation of Upper Pannonian age, while basalt of the same age (Tapolca Basalt Formation) can also be found in the surrounding area (GEOHIDROTERV Kft. 2017). This location was chosen because an earlier survey of MTB diversity in the region (Pósfai & Arató 2000) found here a large variety of morphological types. The artificial pool is exposed to precipitation and the accumulation of natural (e.g., fallen leaves, twigs) and anthropogenic materials (*Fig. 1B*). Ion concentrations in Kinizsi-spring were measured by Tóth (2018): measured in mg/l, the concentrations were 86 for Ca^{2+}, 42 for Mg^{2+}, 13 for Na^{+}, 30 for K^{+}, 440 for HCO_3^{-}, 50 for SO_4^{2-} and 26 for Cl^{-}. The sediment was collected from under a pipe that drains the springwater into the pond, on three occasions, in different seasons (*Table I*). A glass jar was immersed in the basin and filled with sediment and water in approximately equal proportions. Sterilization typically used in microbiological protocols (e. g., with an autoclave) was not implemented; the jars were washed with hot water before sample collection.

Since a laboratory incubator was not applied, the environment (e.g., humidity, temperature) throughout the experiment was not precisely controlled. Glass jars with sediment and water, sealed with their lid, were stored without mixing, on a laboratory shelf at room temperature (~20–23 °C). Intermittently, artificial lighting was used but jars were protected from direct sunlight. MTB were enriched in two steps. First, a bar magnet was placed next to the jar (with its north pole next to the glass), a few mm above the sediment/water interface. The rationale behind this magnet positioning lies in that most MTB cells in the Northern Hemisphere are „north-seekers", i.e., they follow the magnetic field lines downwards, away from toxically high oxygen levels. With this technique MTB that perform „polar magnetotaxis" can be collected (Frankel et al. 1997). After waiting for two hours, the inner wall of the glass next to the magnet (where MTB gathered) was scraped with the tip of a pipette. Then a few ml of sample from this particular spot was pipetted into a round-bottom flask, modified with a "beak". This vessel was filled with MilliQ water up to the "beak" part, and again a bar magnet was placed to the opening of the „beak". With this procedure we made sure that no sediment particles were collected with the cells. After 1 hr, a few ml of the sample – collected in the "beak"– were pipetted and dropped onto a Cu TEM support grid and let to dry before TEM study. One TEM grid was prepared per every observation, i.e., for each magnetic enrichment and cell collection event.

By sampling the pond in different seasons (autumn 2023, spring 2024, winter 2025), we wished to understand whether the dominance of any of the characteristic MTB strains changes over a year. In addition, we also checked whether

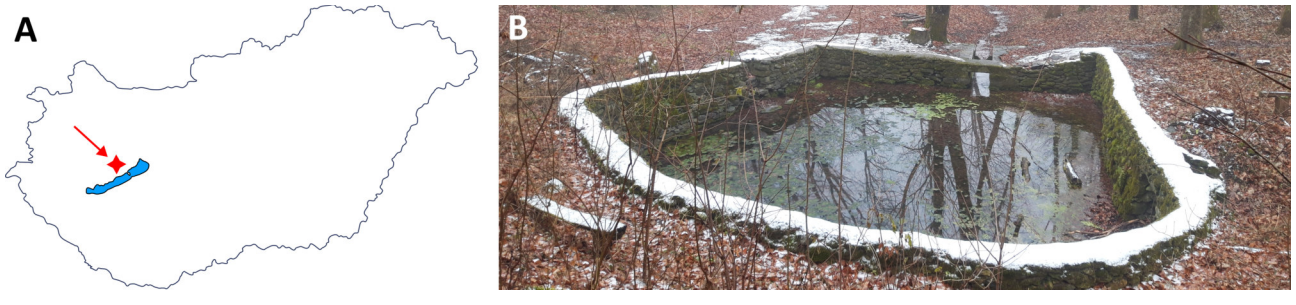


Figure 1. (A) Location of the sampling site (Nagyvázsony, marked in red) in the map of Hungary, and (B) the artificial pool of Kinizsi-spring during winter.
1. ábra. *(A) A mintagyűjtés helye (Nagyvázsony, pirossal jelölve) Magyarország térképén, (B) a Kinizsi-forrás mesterséges medencéje téli időszakban.*

Table I. Sampling dates (in three different seasons) and dates of TEM analyses of samples collected during a given season.

I. táblázat. *A mintavételezések időpontjai (három különböző évszakban) és az adott évszakban gyűjtött minta TEM vizsgálatainak időpontjai.*

	Date of sample collection from Kinizsi-sping		
	23th October 2023	27th April 2024	23th January 2025
Date of TEM measurements	24th October 2023 1st February 2024 2nd May 2024	9th May 2024 12th December 2024	24-29th January 2025 – A →D 10-13th March 2025 – A →D 7-11th April 2025 – A →D 5-8th May 2025 – A → D

'microcosms' – sample jars stored in the lab – show changes over time. The sediment+water sample collected in January 2025 was divided into four equal volumes (marked with the letters 'A', 'B', 'C' and 'D'), and MTB were enriched from the four microcosms on 4 occasions over a period of 4 months (*Table I*). While the four subsamples did not behave uniformly, some general conclusions could be drawn from this experiment.

MTB collected from both fresh and stored samples and the sediment of the 'D' subsample of the material collected in January 2025 were studied using various transmission electron microscopy (TEM) techniques, using a Talos F200X scanning transmission electron microscope at 200 kV accelerating voltage, equipped with a four-detector energy-dispersive X-ray spectrometer (EDS). High-angle annular dark-field scanning transmission electron microscopy (STEM HAADF) was mostly used for imaging. The elemental composition of the cells and the sediment were obtained from STEM EDS element maps using Thermo Scientific Velox Software version 3.15, the extracted data were collected and plotted in Microsoft 365 Excel. In addition, electron tomography (ET) was also performed on cells from the October 2023 sample, in order to study the positions of magnetosomes and other inclusions within cells. During tomographic data collection, a tilt series of STEM HAADF images was taken in the tilt range of -68 to +75 degrees (tilt step was 1°). Then a 3D morphological reconstruction was calculated from the obtained 144 images. Inspect 3D software was used for 3D reconstruction and segmentation, 3D visualization was performed using the Dragonfly 3D software (Comet Technologies Canada Inc.).

In addition to STEM HAADF imaging, X-ray powder diffraction (XRPD) was used to study the sediment of the 'D' subsample of the sample collected in January 2025. XRPD measurements were performed using a Philips PW3710 instrument, using $Cu_{K\alpha}$ radiation, at an accelerating voltage of 50 kV and a current of 40 mA, in the angular range of 4–70° 2Θ with a step size of 0.02. The sample was powdered in agate mortar under ethanol and deposited onto a glass plate.

Results

During one of our sampling events (January 2025), some basic data about the springwater were measured. The pH of the 9 C water was 7.47; the dissolved oxygen level was 12.32 mg/l and electrical conductivity (EC) was 540 μS/cm.

In any of the freshly collected samples we observed a large diversity of MTB cell types. Since no microbiological characterization was performed, we distinguished the characteristic MTB strains on the basis of features observable using TEM: cell morphology (vibrio, coccus, spirillum, rod), types of magnetosome chains (single, double, double-double, scattered), magnetite morphologies (cubooctahedral, 'prismatic', 'ladyfinger', and 'bullet'), and types of inclusions (polyP, S, ACC). Based on these features, we distinguished several MTB cell types in any sample, among which eight were present in all samples, which are the focus of our study (*Table II* and *Figs 2* and *3*).

Most of the studied bacterial cells are approximately 2–3 m in diameter (*Figs 2* and *3*). Rod-shaped bacteria containing bullet-shaped magnetite particles (R1B) are slightly larger, approximately 4–6 m long and do not contain any other inclusions. Concerning the distribution of various inclusions in the identified MTB cell types, some general observations were made.

Table II. MTB cell types present in the samples, categorized by cell morphology, magnetosome chain structure, magnetite morphology, and inclusions.

II. táblázat. *A mintákban előforduló sejttípusok sejtmorfológia, magnetoszóma lánc, magnetitmorfológia és a bennük előforduló zárványok alapján.*

	MTB types present in the samples							
Cell type	*coccus*	*coccus*	*coccus*	*coccus*	*vibrio*	*spirillum*	*rod*	*rod*
Chain	single	two single	two double	scattered	single	single	single	single or multiple
Magnetite morphology	prism	prism	prism	ladyfinger	prism	prism	prism	bullet
Inclusion	none or S	polyP,S	polyP	polyP, S	none, ACC,S	ACC	polyP	none
Identifier	C1P	C2P	C22P	CSL	V1P	S1P	R1P	R1B

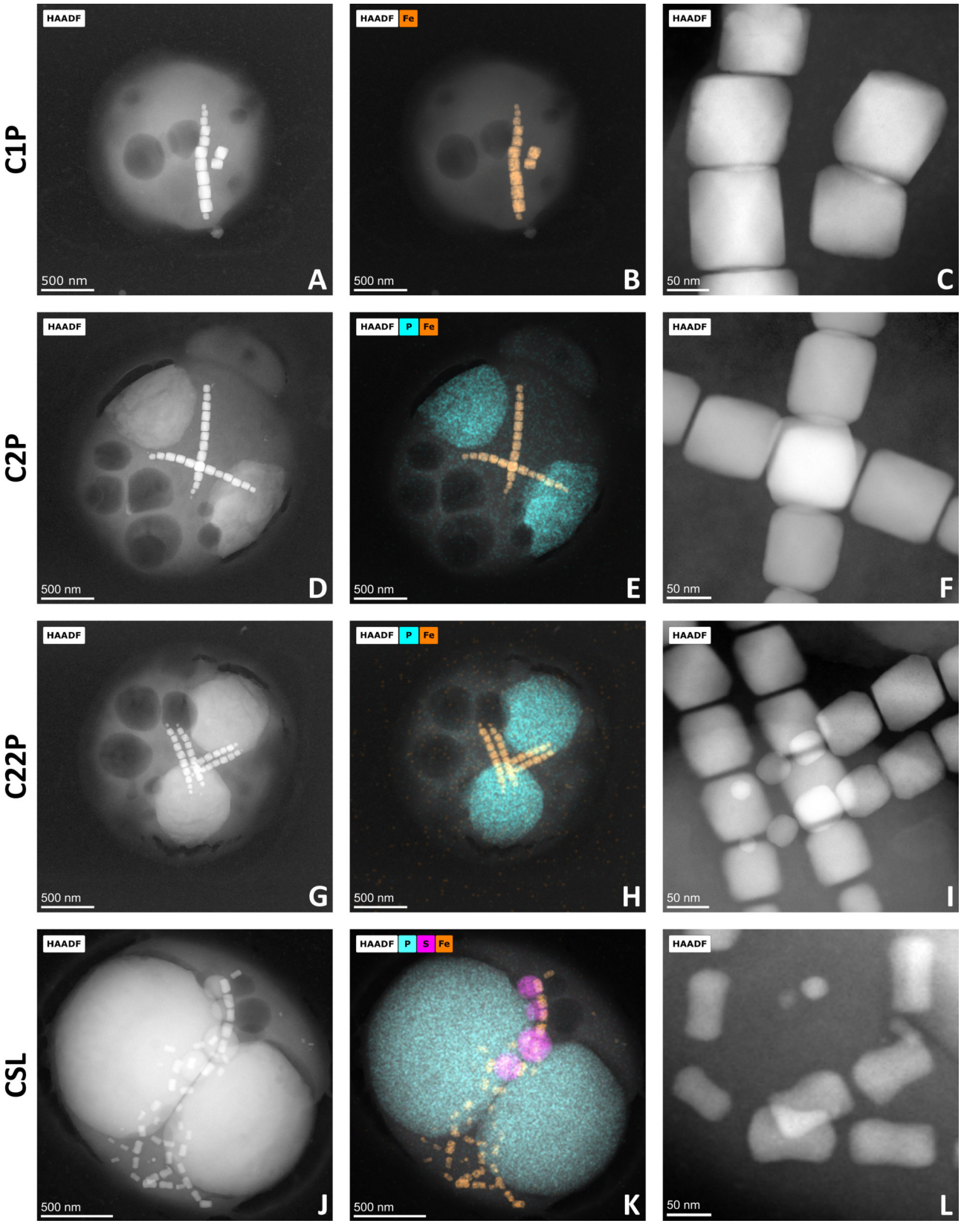


Figure 2. Four distinct MTB cell types from Kinizsi-spring (C1P, C2P, C22P and CSL, see *Table II*). Left column of panels (A, D, G, J): STEM HAADF images of MTB cells; middle column (B, E, H, K): EDS element maps of the same cells, indicating the presence of S, P and Fe; right column (C, F, I, L): magnified HAADF images of magnetite crystals in the particular cell (C, F, I: 'prism', L: ladyfinger-shaped crystals).

2. ábra. *A Kinizsi-forrásból azonosított négy különböző MB sejttípus (C1P, C2P, C22P és CSL, lásd* II. táblázat*). Bal oldali oszlop (A, D, G, J): a sejt STEM HAADF-felvétele; középső oszlop (B, E, H, K): az adott sejt S, P, Fe EDS-elemtérképe; jobb oldali oszlop (C, F, I, L): a sejtben található magnetit kristályokról készített, nagyobb nagyítású HAADF-felvétel (C, F, I: 'prizma', L: babapiskóta alakú kristályok).*

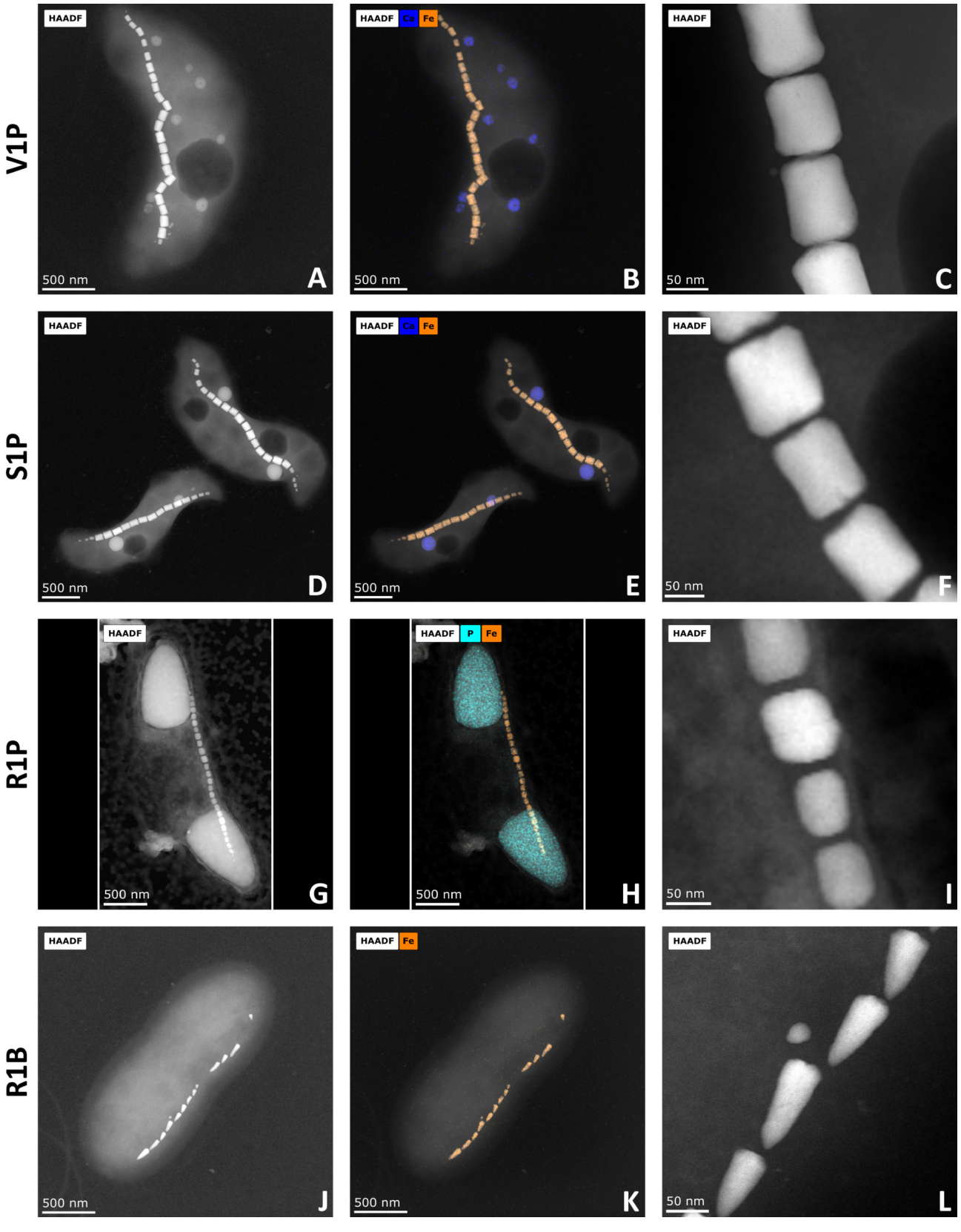


Figure 3. Additional four distinct MTB cell types from Kinizsi-spring (V1P, S1P, R1P and R1B, see *Table II*). Left column of panels (A, D, G, J): STEM HAADF images of MTB cells; middle column (B, E, H, K): EDS element maps of the same cells, indicating the presence of Ca, P and Fe; right column (C, F, I, L): magnified HAADF images of magnetite crystals in the particular cell (C, F, I: 'prism', L: 'bullet'-shaped crystals).

3. ábra. *A Kinizsi-forrásból azonosított további négy különböző MB sejttípus (V1P, S1P, R1P és R1B, lásd* II. táblázat*). A bal oldali oszlopban (A, D, G, J) a sejt STEM HAADF-felvétele; a középsőben (B, E, H, K) az adott sejt Ca, P, Fe EDS-elemtérképe; a jobb oldaliban (C, F, I, L) a sejtben található magnetit kristályról készített HAADF-felvétel látható (C, F, I: 'prizma', L: 'lövedék' alakú kristályok).*

PolyP granules

C2P, C22P, CSL and R1P cell types typically all had polyP inclusions (*Fig. 2E, H, K* and *Fig. 3H*). Whereas most C2P, C22P and R1P cells displayed two polyP inclusions of medium size (relative to the cell diameter), CSL cells in many samples contained gigantic polyP inclusions that appeared to fill almost the entire cytoplasm (*Fig. 2K*). C2P cells were rarely present in the collected samples. According to electon diffraction patterns, polyP inclusions were amorphous. Elemental compositions of R1P cells' polyP granules were not studied, since such cells rarely occurred. Since C22P and CSL were the most abundant cell types in the majority of samples, we focused on these two types. Because of the large size of polyP inclusions in some cells, we wished to determine the amount of P (relative to C) (*Fig. 4B*). In addition, since the concentrations of minor elements in polyP inclusions have never been analyzed in MTB, and rarely in any other microorganisms (Rácz et al. 2026), we determined the compositions of polyP inclusions in these two cell types (*Figs 4A* and *S1*).

P/C ratios of the two types of cocci differed (*Fig. 4B*). The data points for CSL showed greater dispersion, as their polyP granules varied in size. If a cell contained more than one polyP inclusion, the mean from all polyP granules within the cell was calculated for each element (*Figs 4A* and *S1*). PolyP inclusions in CSL had higher P and Mg, and lower Ca than in C22P cells.

S granules

S granules occurred in C1P, C2P, CSL and V1P cells (*Figs 2A, D, J* and *3A*). The 'A' jar from the sample collected in 2025 January contained S granules (in C1P cells) most abundantly. S granules varied in size, with an average diameter of ~600 nm in the 'A' jar of sample 2025 January, but smaller ones were also found in other samples. The compositions of 20 S inclusions were analyzed using STEM-EDS. Apart from biogenic elements (C, N, O), probably contributed to the spectra by the cellular background, the analyzed grains contained 0 to 2 at% of other elements (including Na, Mg, P, Cl, K, Ca). Thus, S inclusions practically consist of elemental S.

ACC granules

Amorphous calcium carbonate (ACC) granules occurred in V1P and S1P cells (*Fig. 3B, E*). Even these cell types rarely contained such inclusions. Since ACC particles were rather small (on average 139 nm in diameter), and only a few tens were observed, a statistical evaluation of their compositions was not possible. Nevertheless, it could be ascertained that Ca was the only alkaline earth cation present with a concentration exceeding the detection limit of EDS.

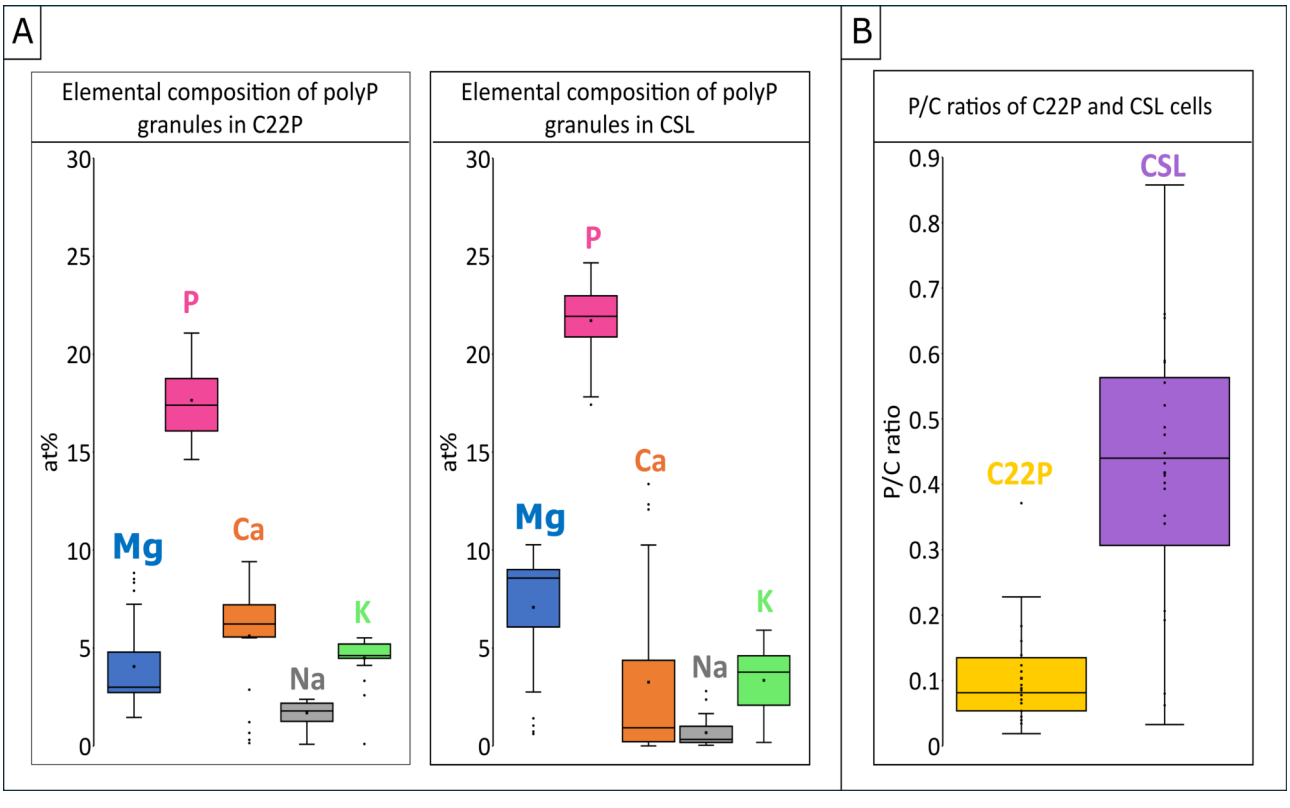


Figure 4. (A) Elemental composition of polyP granules in C22P and CSL cells (C, O and N are not included in the analysis). (B) P/C molar ratios of C22P and CSL cells. Experimental data obtained from STEM EDS maps are shown without the removal of contribution of signals by the cellular background.

4. ábra. *(A) C22P és CSL sejtek poliP zárványainak elemi összetétele (C, O, N nélkül). (B) C22P és CSL sejtek P/C mólarányai. Az ábrázolt adatok STEM EDS-elemtérképek alapján, a sejthátterből adódó jel kivonása nélkül készültek.*

Positions of cellular inclusions

It is of interest how the various intracellular organelles are packed into the cell, since the magnetically guided movement of the cell might be affected by the distribution of large inclusions that are relatively heavier than the cytoplasm. We used STEM HAADF ET to study the 3D arrangement of intracellular organelles. From a technical point of view, MTB played an important role in the development of STEM HAADF ET, since the first applications of the technique

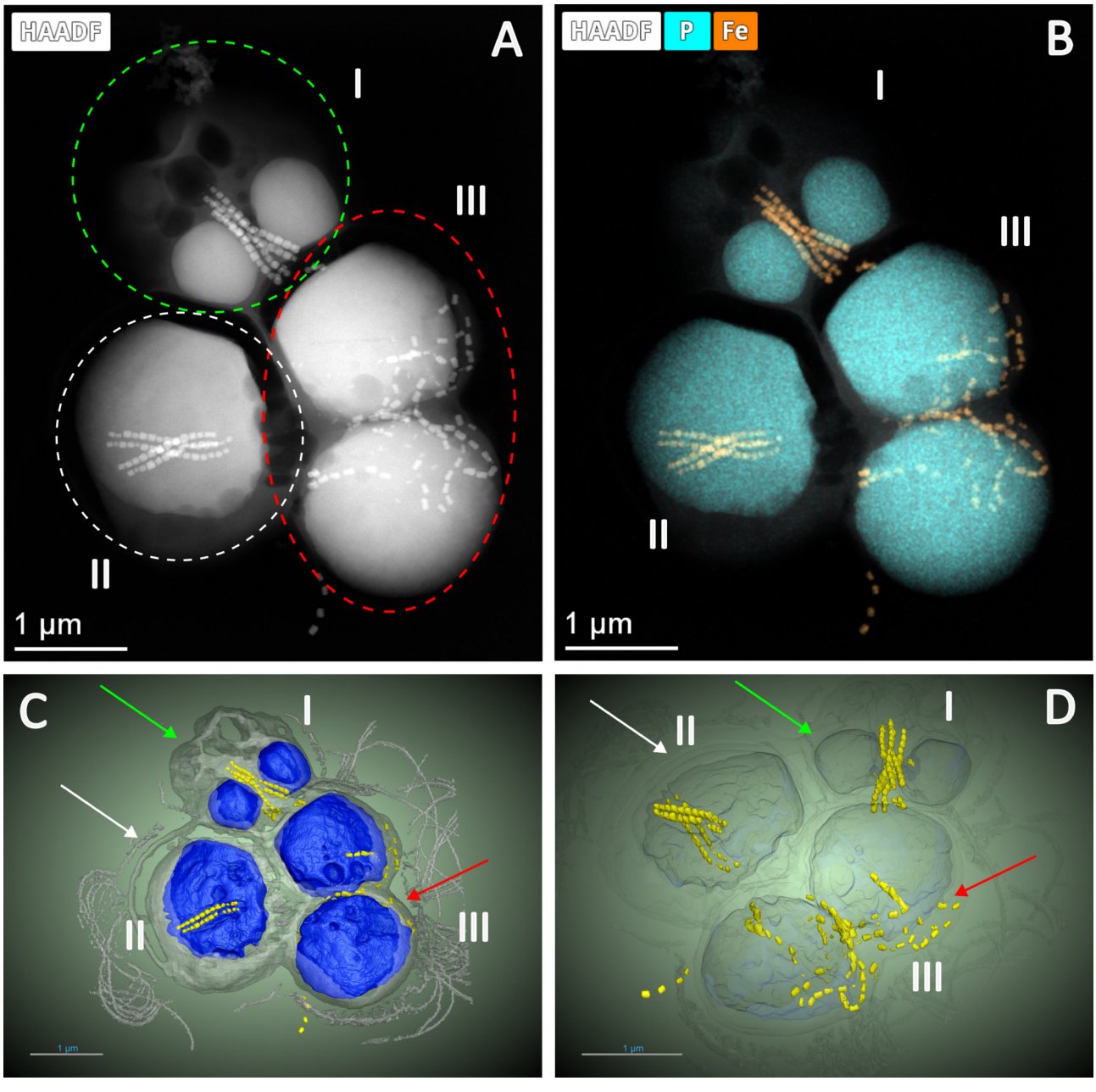


Figure 5. Electron tomographic analysis of the spatial distribution of intracellular inclusions in an aggregate consisting of three MTB cells, from the October 2023 sample. (A) STEM HAADF image, the dashed lines in different colors mark the boundaries of the three cells: two C22P-type (I and II) cells and one CSL-type (III) cell. (B) composite of a STEM HAADF image and EDS elemental maps: P (turquoise) shows the polyP granules, Fe (orange) shows the magnetite chains. (C) A visualization of the 3D reconstruction, based on electron tomography, of the aggregate of the three MTB cells. The cells are shown with their flagella in grey, each with polyP inclusions (blue) and chains of magnetite crystals (yellow). One of the C22P cells (green arrow, I) contains two smaller, the other cell (white arrow, II) one large, whereas the CSL cell (red arrow, III) two large polyP inclusions. (D) Positions of magnetite chains inside cells. In the two C22P cells (I and II) the double magnetosome chains form an X-shape; in the CSL cell (III) short chain segments occur. Dragonfly 3D software was used for 3D visualization.

5. ábra. *Sejtzárványok térbeli helyzetének elektrontomográfiás elemzése egy három mágneses sejtből álló aggregátumban (2023. októberi minta). (A) STEM HAADF-felvétel, melyen a különböző színű szaggatott vonalak az egyes sejtek határait jelzik: két C22P (I és II) és egy CSL (III) típusú sejt. (B) STEM HAADF-felvétel és EDS-elemtérképek kompozitja: a P jel (türkiz) a polifoszfát szemcséket, az Fe jel (narancssárga) a magnetitláncokat jelöli. (C) A három MB sejt aggregátumáról elektrontomográfia alapján készült 3D rekonstrukció egy vizualizációja. Mindhárom sejt flagellumaival (szürke), poliP zárványaival (kék) és magnetitláncaival (sárga) együtt látható. A zöld nyíllal jelölt C22P sejtben (I) két kisebb, a fehér nyíllal jelölt C22P sejtben (II) egy nagyobb, a piros nyíllal jelölt CSL sejtben (III) két nagy poliP zárvány van. (D) A magnetitláncok sejten belüli elhelyezkedése. A két C22P sejtben (I és II) a két dupla magnetitlánc X-alakban helyezkedik el; a CSL sejtben (III) rendezetlen magnetitlánc-darabok láthatók. A 3D vizualizációhoz a Dragonfly 3D szoftvert használtuk.*

used MTB with their magnetosome chains as test objects (KASAMA et al. 2006, WEYLAND et al. 2006, LI et al. 2015).

Since the cells dried on the specimen support film and were imaged under high-vacuum conditions, their original state was not preserved: their water content evaporated, and the presumably spherical polyP granules look flattened. Nevertheless, we believe that the relative arrangement of magnetosome chains and intracellular inclusions was preserved.

In the ET-based 3D reconstruction of two C22P cells (marked I and II) and one CSL cell (marked III) (from the October 2023 sample) polyP granules appear to fill most of the cell volume (*Fig. 5*; and supporting video about the 3D reconstruction of the cells: https://youtu.be/RU-7zKK8P2M). Double magnetosome chains form an X-shape in projection, and the two pairs of chains are located under one another. In the case of cell II a large polyP granule is sandwiched between the two double chains (best seen in the video). The flagellar bundles originate from a point near the extension of the double magnetosome chains. In the CSL cell (marked III) short chain segments can be identified, some of which run between the two large polyP inclusions, while others cluster at one side of the cell, where flagellar bundles appear to be anchored. Thus, in both types of cells the flagella are positioned in accordance with the magnetic moment of the cell, with the flagellar motors presumably symmetrically arranged relative to the cellular dipole, ensuring that their rotation will propel the cell parallel to its magnetic moment.

Seasonal changes in MTB cell types and their inclusions in freshly collected samples

Seasonal changes in the abundance of distinct cell types were studied in TEM specimens from magnetic enrichments prepared immediately after three sample collections (in October 2023, April 2024, and January 2025 – see *Table I*). The changes of cell types over time are illustrated by *Figure 6*.

The October 2023 sample contained all cell types discussed above but C1P and CSL were dominant (*Fig. 7*). The April 2024 sample had similar cell types, with a dominance of CSL (*Fig. 8*). Many cells contained polyP particles but they were smaller relative to the cell size than the ones in the October sample. C1P cells also occurred. Interestingly, some cells had Ca-bearing, probably ACC shells (*Fig. 8B*). The January 2025 sample was clearly dominated by C1P cells, with a spectacularly large number of S inclusions (*Fig. 9*).

Previous observations suggested that when MTB 'microcosms' are stored in the lab, certain strains may become dominant over others (FLIES et al. 2005, KÓSA & PÓSFAI 2007). In order to better understand the cycling of P and S by MTB, we stored the original samples in the lab and sampled after several months (*Fig. 6*).

The original October 2023 sample was studied again in February 2024. By then CSL cell types were dominant with minor spirilla and vibrio also present (*Figs 6* and *10A*). By May 2024 the same sample looked entirely different: distinct clusters consisting of almost exclusively C22P cell types with large polyP granules (*Figs 6* and *10B*), as well as clusters of the same cell type with holes in places of their consumed polyP granules occurred (*Fig. 10C*).

The April 2024 sample was studied again after more than half a year, in December 2024. Surprisingly, this sample was dominated by previously unseen, rod-shaped cells with elongated polyP granules at both ends (R1P type) (*Figs 6, 11*).

The sample collected in January 2025 was divided into four subsamples (A, B, C, and D), in order to study whether the previously observed changes in the microcosms were entirely random or they follow a certain pattern. All four subsamples were repeatedly examined 1, 2, and 3 months after sample collection (*Fig. 6*). While subsamples A, C, and D produced broadly similar changes, subsample B behaved in a different way: after one month the V1P cell type (vibrio with prismatic magnetosomes, with or without S or ACC inclusions) became dominant, and this cell type remained present until the end of the experiment.

In subsample A initially C1P cells with S inclusions were by far the largest contributors to the MTB pool (*Fig. 12A*). More than a month later CSL cells with medium-sized polyP granules dominated, with many cells exhibiting Ca-bearing shells (*Fig. 12B*). After more than two months, the CSL cells were still most common (*Fig. 12C*).

Since subsamples C and D showed almost identical changes, the results from only C are shown (*Fig. 12*). In the fresh subsample there were much fewer S granules than in A (*Fig. 12D*). More than a month later, practically all cells contained polyP granules: CSL and R1P cells were present (*Fig. 12E*). After more than two months, R1P cells became the largest fraction of the MTB consortium and they dominated by the end of the experiment (*Fig. 12F*).

Composition of the sediment

In October 2026, XRPD and STEM HAADF imaging were performed about the sediment of the 'D' subsample of the sample collected in January 2025 (*Figs S2, S3*). XRPD data show that quartz, carbonates (calcite and dolomite) and silicates (albite, orthoclase and muscovite) occur in the sample. (*Fig. S2*). Consistent with XRPD results, STEM EDS maps also indicate the presence of carbonates and silicates (*Fig. S3*). The sample also contains nanoparticles of titanium dioxide that were not detected by XRPD. In addition, both iron oxide and iron sulfide occur, suggesting that particles from both oxic and anoxic microenvironments of the sediment were collected. The mineralogical identity of these phases was not determined.

Discussion

The consistent association between inclusion type and other cellular traits (*Table II* and *Figs 2, 3*) suggests that the formation of non-magnetic inclusions in the Kinizsi-spring MTB is not merely a passive response to local chemistry, but

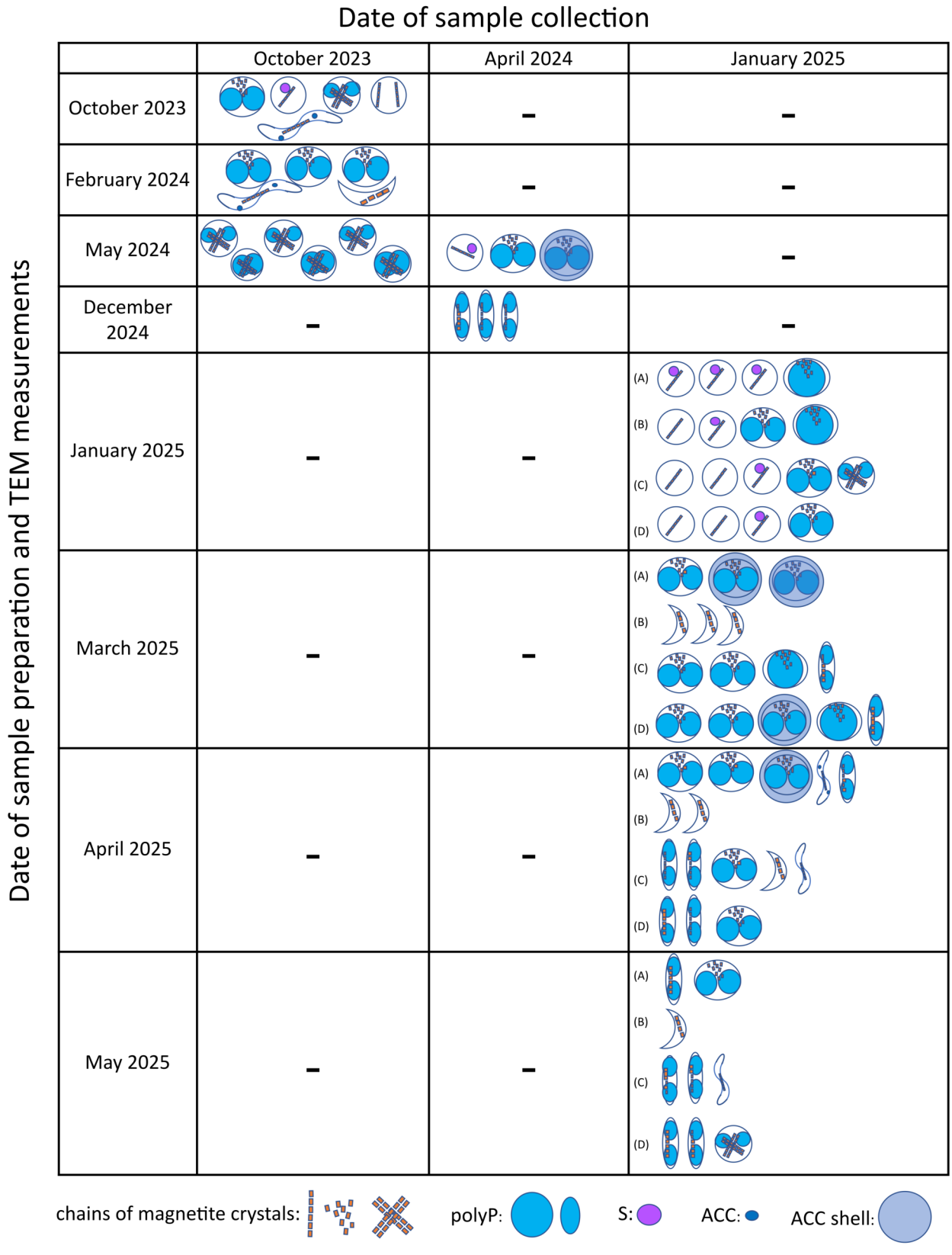


Figure 6. Schematic illustration of MTB cell types observed in samples that were collected in different seasons (autumn 2023, spring 2024, winter 2025). A sample collected in January 2025 was divided into four equal parts and studied monthly until May 2025. "–" : no TEM measurement performed during that month. Drawings of the different cell types are for illustrative purposes only. The number of identical cells in each sample visually represents the estimated quantity of a certain MTB cell type; however, a statistical analysis of cell type ratios was not performed.

6. ábra. *Különböző évszakokban (2023. ősz, 2024. tavasz, 2025. tél) vett mintákban azonosított MTB sejttípusok sematikus ábrái. A 2025. január végén gyűjtött, 4 részre osztott mintát 2025 májusáig havonta elemeztük. „ – ": a jelölt időszakban nem történt TEM-vizsgálat. A különböző sejttípusok sematikus rajzai illusztratív jellegűek. Az azonos sejtek száma vizuálisan reprezentálja a mintákban lévő MTB sejtek becsült mennyiségét, de statisztikai elemzés nem készült a pontos arányokról.*

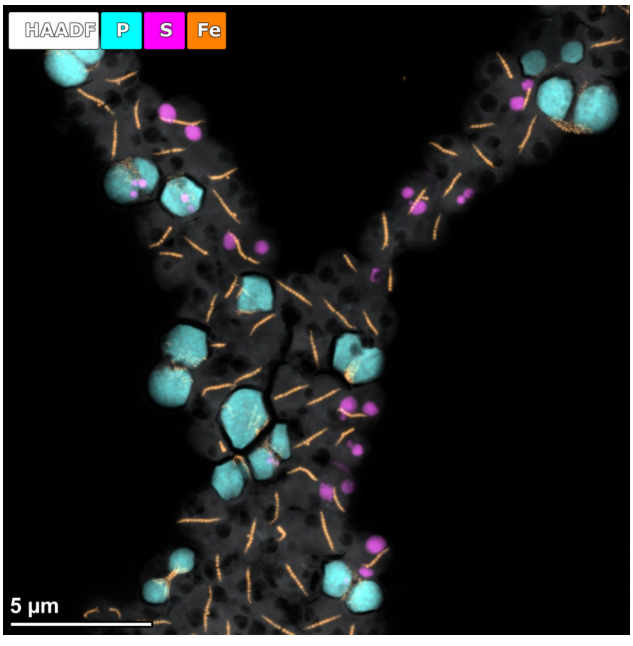


Figure 7. A typical cluster of MTB cells from the fresh October 2023 sample (composite of HAADF image and EDS element maps). Mostly C1P and CSL cell types, with many of the C1P cells without any polyP or S inclusions.

7. ábra. *MTB sejtek jellegzetes halmaza a friss 2023. októberi mintában (HAADF-felvétel és EDS-elemtérkép kompozitja). Nagyrészt C1P és CSL típusú sejtek láthatók, a C1P sejtek zöme nem tartalmaz polyP vagy S zárványt.*

is at least partly under genetic control. In our samples, polyP, S and ACC inclusions are not randomly distributed among all cells; rather, they are linked to reproducible combinations of cell morphology, magnetosome-chain configuration and magnetite crystal morphology. Thus, ACC occurs mainly in spirilla and, more rarely, in vibrios, whereas polyP-rich inclusions are characteristic of several coccoid and rod-shaped morphotypes, and elemental S occurs in specific cocci and vibrios. This pattern parallels the well-established species- or strain-specific control of magnetosome biomineralization, in which magnetite crystal morphology and chain organization correlate with phylogeny and magnetosome gene content (Pósfai et al. 2013; Liu et al. 2021, 2023). By analogy, the repeated coupling of inclusion type with the broader cellular phenotype in the Kinizsi-spring assemblage indicates that the capacity to produce polyP, S or ACC is probably encoded in lineage-specific metabolic and biomineralization programs, even if the size and abundance of inclusions may vary with environmental conditions.

This interpretation is consistent with recent genomic and microscopic studies of MTB inclusions. Li et al. (2021) showed that a single freshwater magnetotactic spirillum can form S globules and Ca/Mg-rich polyP granules in addition to magnetosomes, but that these inclusions occur only in a subset of cells, implying that they are temporary storage or transport structures whose formation depends on both genotype and physiological state. For intracellular carbonates, Liu et al. (2025) identified calcifying MTB and showed that their carbonate inclusions contain selectively accumulated, other divalent cations.

In the case of polyP and S, the cultivated freshwater coccus FCR-1 isolated from Chichijima, Japan, provides a useful comparison: it forms polyP granules under growth conditions typical of the oxic-anoxic transition zone, while S granules appear during chemolithoautotrophic growth with

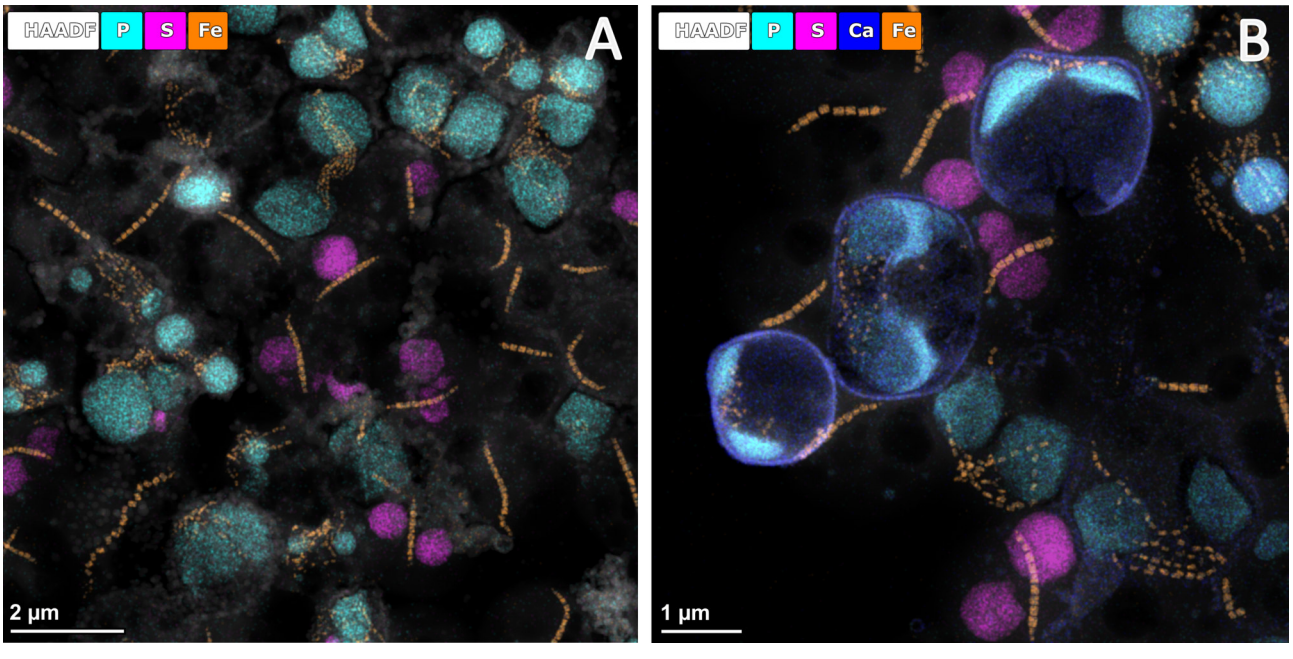


Figure 8. (A) A group of MTB cells from the fresh April 2024 sample (composite of HAADF image and EDS element maps). Primarily CSL cells with large polyP inclusions, and C1P also occur. (B) Ca-bearing shells around CSL cells.

8. ábra. *(A) MTB sejtek a friss 2024. áprilisi mintában (HAADF-felvétel és EDS-elemtérképek kompozitja). Főleg CSL sejtek, nagy poliP zárványokkal, és C1P sejtek is előfordulnak. (B) Ca-tartalmú burok a CSL sejtek körül.*

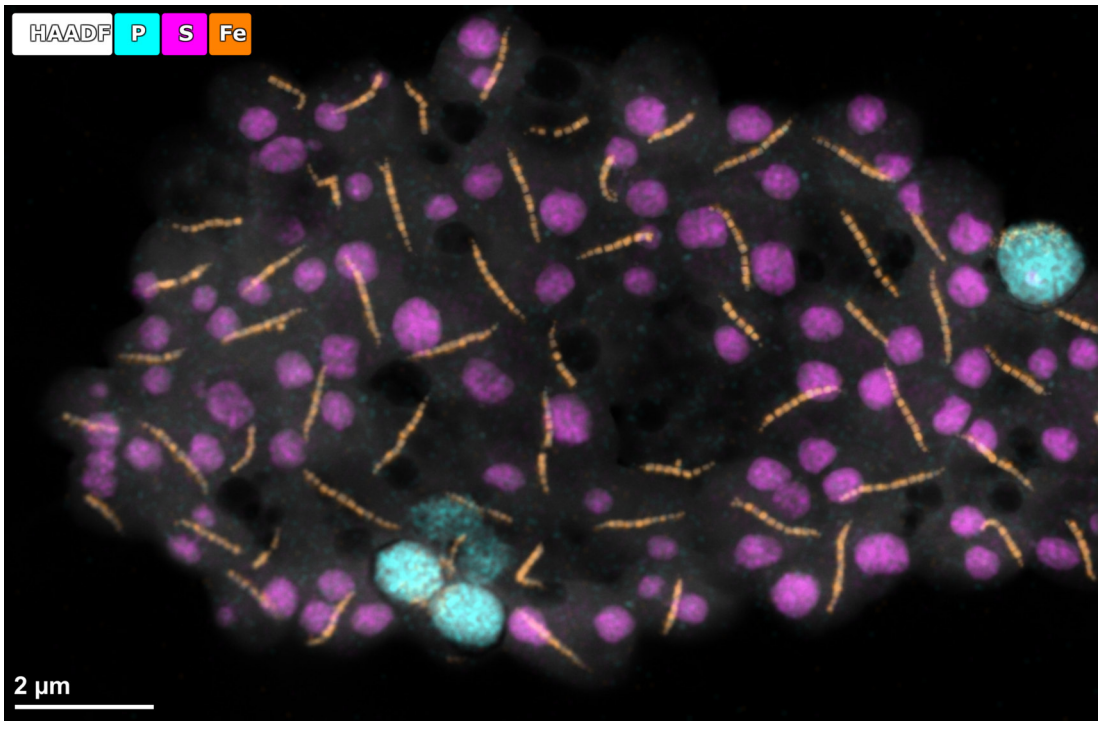


Figure 9. Predominantly C1P cells with S granules in the fresh January 2025 sample (composite of HAADF image and EDS element maps).
9. ábra. *Túlnyomórészt C1P sejtek S zárványokkal a 2025. januári friss mintában (HAADF-felvétel és EDS-elemtérképek kompozitja).*

sulfide as the electron donor (SHIMOSHIGE et al. 2025). Together, these observations imply that inclusion production in MTB is best viewed as genetically constrained but environmentally modulated: the genome determines which intracellular mineral or storage system a given strain can deploy, whereas redox state, sulfide, phosphate and carbonate/cation availability regulate when and to what extent the inclusions are expressed.

The most direct evidence for a biogeochemical role of polyP-bearing MTB comes from stratified water columns where the oxic-anoxic transition zone is expanded over metres to tens of metres and can therefore be sampled with high vertical resolution. According to SCHULZ-VOGT et al. (2019), in the Black Sea the dissolved phosphate profile displays a distinct minimum at the upper boundary of the suboxic zone and a maximum at the lower boundary. SCHULZ-VOGT et al. (2019) argued that magnetotactic cocci (of approximately 5 µm in diameter) can account for this "phosphate shuttle" by taking up phosphate near the upper boundary, storing it intracellularly as polyP, and releasing phosphate deeper in the suboxic zone through polyP degradation. This mechanism is made plausible by magnetotaxis itself: by moving up and down across the oxic/anoxic interface, MTB can repeatedly cross the zone in which phosphate, nitrate, sulfide and oxygen availability change sharply (SCHULZ-VOGT et al. 2019).

Lake Pavin provides an important freshwater analogue (BIDAUD et al. 2022), even though it has a limnological character distinct from Kinizsi-spring (RIVAS-LAMELO et al. 2017).

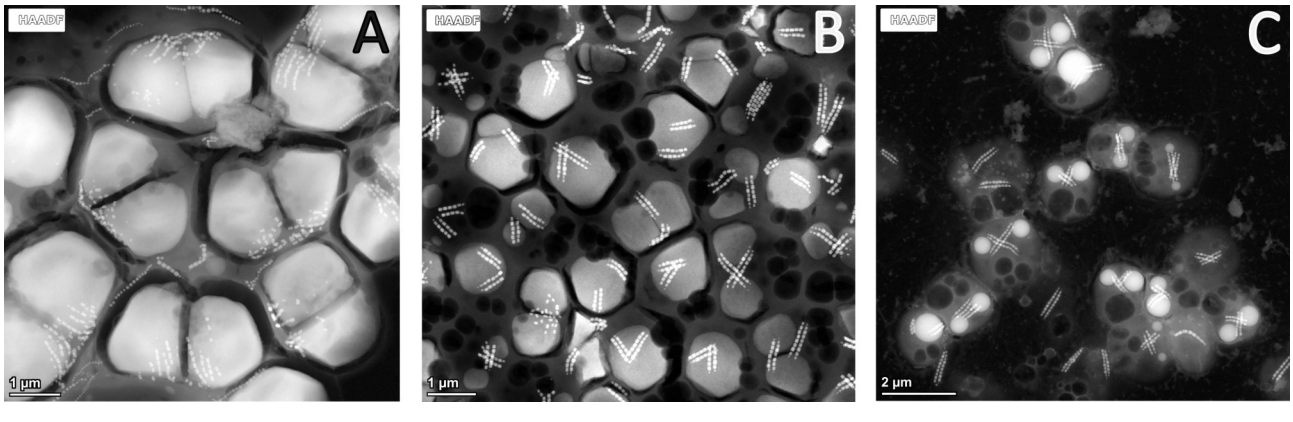


Figure 10. October 2023 sample stored in the lab and studied after (A) four and (B, C) seven months. (HAADF images.)
10. ábra. *A laborban tárolt 2023. októberi minta (A) négy és (B, C) 7 hónap elteltével. (HAADF-felvételek.)*

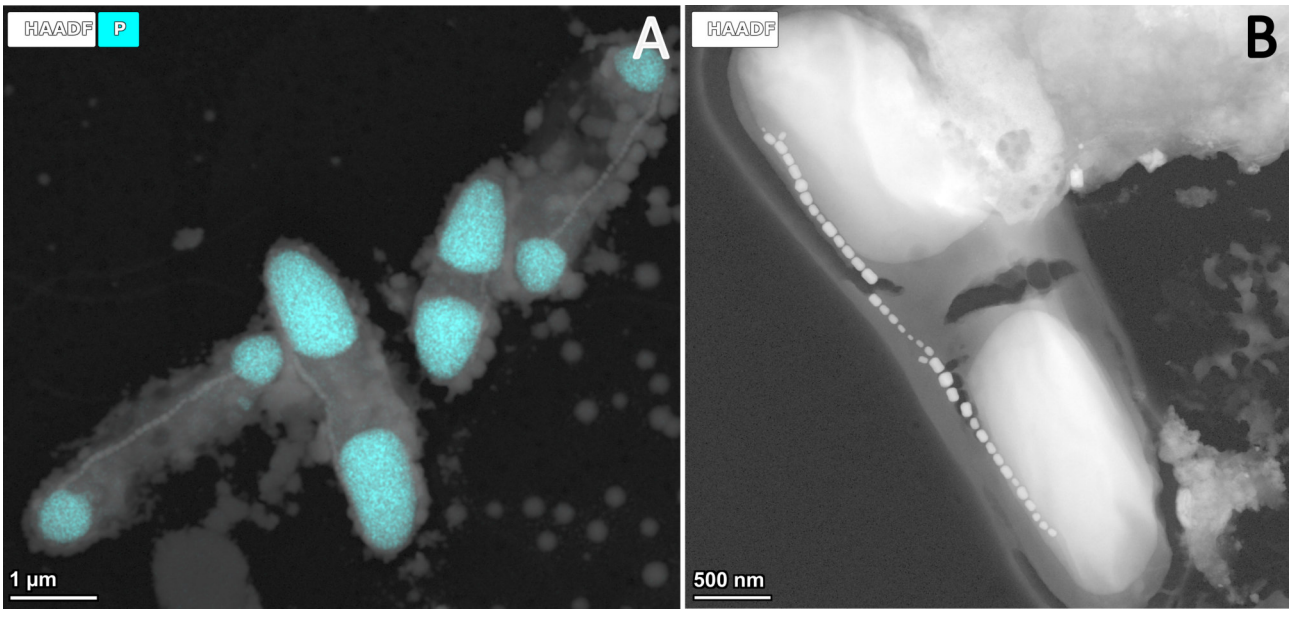


Figure 11. R1P-type cells in the April 2024 sample that was stored in the lab and studied after 7 months. (A) Four cells, composite of HAADF image and P element map, (B) HAADF image of a cell that contains two large (relative to the cell) polyP inclusions.

11. ábra. *R1P típusú sejtek a laborban tárolt 2024. áprilisi mintában, mintavétel után 7 hónappal. (A) Négy sejt HAADF-képének és P-elemtérképének kompozitja, (B) két, a sejt méretéhez képest óriási poliP zárványt tartalmazó sejt HAADF-felvétele.*

In Lake Pavin, magnetotactic cocci can contain massive polyP inclusions, in some cases occupying most of the cell volume, similar to the CSL cell types observed in Kinizsi-spring. Since cocci are spherical and thus have the smallest surface to volume ratio among the various morphological cell types, it is the easiest for them to maintain cellular activities and to aquire and store elements from the environment. In Lake Pavin these cells occur below the oxic-anoxic transition zone in a ferruginous, poorly sulfidic water column (Rivas-Lamelo et al. 2017, Bidaud et al. 2022). The association between magnetotactic cocci, particulate phosphorus and redox gradients suggests that such organisms can act as mobile phosphorus reservoirs. In MTB, magnetic navigation allows repeated positioning within narrow chemical niches, and polyP accumulation can occur even in anoxic portions of the water column. This is relevant for the Kinizsi-spring microcosms because the sediment-water jars likely developed steep, dynamic redox and nutrient gradients. Under such conditions, polyP-rich cocci and rods may not simply indicate high ambient phosphate; rather, their abundance may reflect intervals when motile MTB shuttle between microoxic and anoxic microniches, alternately acquiring, storing and remobilizing phosphorus.

The possible function of ACC inclusions is less well constrained than that of polyP, but the available observations suggest that they are not incidental precipitates. In MTB from Lake Pavin and other freshwater systems, intracellular ACC inclusions are lineage-specific, occur together with magnetosomes, and can occupy a large fraction of the cell volume (Rivas-Lamelo et al. 2017, Bidaud et al. 2022). In the Kinizsi-spring material, the ACC inclusions are much smaller and rarer (*Fig. 3*) than the large Lake Pavin examples, so their contribution to bulk carbonate or metal cycling is probably limited. Nevertheless, their preferential occurrence in specific spirillum and vibrio morphotypes supports the view that ACC formation is a genetically enabled physiological trait. In karstic spring environments, where Ca and bicarbonate activities are high, such a trait may provide a selective advantage by linking ion regulation, motility and intracellular biomineralization. The occurrence of an ACC shell around cocci in some samples (*Figs 8B* and *12B*) is a novel observation. We can only speculate that the cells are passively encrusted by ACC in a carbonate/calcium-rich environment.

The temporal shifts observed in the stored Kinizsi microcosms (*Fig. 6*) probably reflect changes in nutrient availability and microbiota-driven redox cycling rather than simple stochastic replacement of one MTB type by another. Laboratory sediment-water microcosms develop steep chemical gradients analogous to natural oxic-anoxic transition zones, where oxygen, nitrate and sulfate supplied from the upper layers and reduced species such as Fe^{2+}, NH_4^+ and sulfide generated below. MTB can exploit these gradients by magnetically guided vertical shuttling, thereby coupling magnetosome formation with Fe, S, P, N and C cycling (Li et al. 2021). In this framework, dominance of S-bearing cocci may indicate periods when sulfide oxidation is favored (in this case in winter) (*Fig. 9*). The increases in polyP-rich cells may reflect phosphate uptake/storage and subsequent release during changing redox conditions (*Figs 6, 12*) and decreasing nutrient availability, since the production of ATP and DNA requires phosphate.

The divergence among replicate winter microcosms (*Fig. 6*), including the sustained dominance of vibrios in one bottle, is therefore not unexpected: small initial differences in sediment composition, organic-matter degradation, micro-

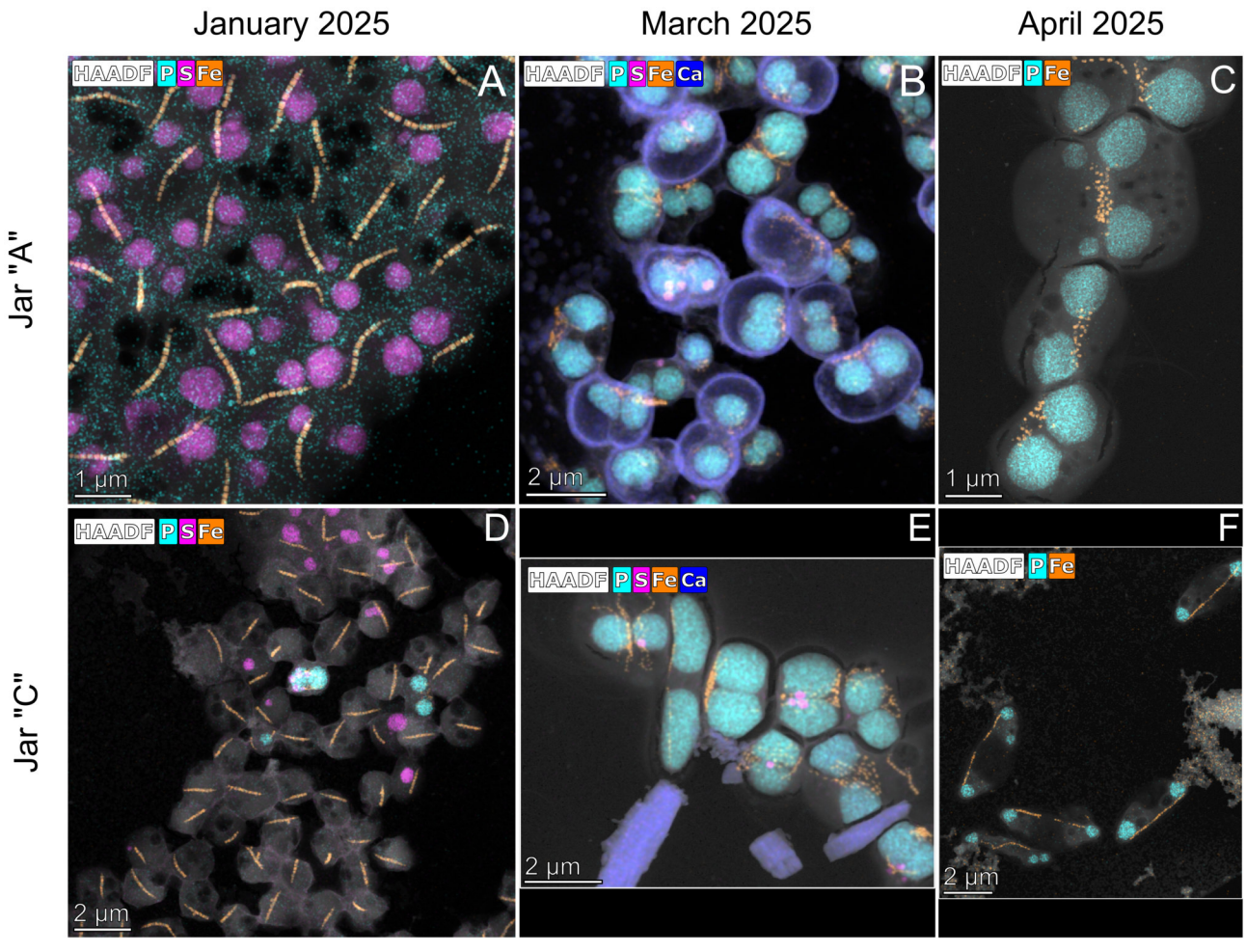


Figure 12. Changes in the dominant MTB cell types in the 'A' and 'C' subsamples of the sample collected in January 2025, studied at three different times (January, March and April 2025). Top row (A, B, C): composites of STEM HAADF images and elemental maps of 'A' microcosm. Bottom row (D, E, F): composites of STEM HAADF images and elemental maps of 'C' microcosm.

12. ábra. *MTB sejttípusok változása a 2025. januári minta 'A' és 'C' mikrokozmoszában, három időpontban vizsgálva (2025. január, március és április). A felső sorban (A, B, C) az 'A' mikrokozmosz, az alsó sorban (D, E, F) a 'C' mikrokozmosz STEM HAADF-felvételeinek és elemtérképeinek kompozitjai láthatók.*

bial competitors and sulfide/phosphate production can shift the chemical niche structure and select different MTB consortia. The observed succession of inclusion-bearing morphotypes (*Fig. 6*) is thus likely to record short-term nutrient and biogeochemical cycles and shifts in microbial composition within the microcosms, rather than seasonal change alone.

The production of polyP inclusions that are huge relative to the cell size, by CSL and C22P morphotypes, raises the possibility of using these strains for magnetically removing phosphorus from aqueous solutions (e.g., wastewater), with a potential for recycling. Although the isolation and subsequent cultivation of CSL, the strain with the most efficient P-enrichment mechanism (*Fig. 4B*), are beyond the scope of our research, we plan to perform experiments with natural MTB consortia from Kinizsi-spring. Since the temporal changes in MTB strains consistently show the development of a dominance of large polyP-bearing cells including CSL, C22P and R1P (*Fig. 6*), we envisage that such consortia could be used in a technological process of magnetically-assisted phosphorus removal.

Conclusion

The MTB assemblages from Kinizsi-spring contain diverse intracellular inclusions, including polyphosphate, elemental sulfur and amorphous calcium carbonate, whose occurrence is closely linked to specific cell morphologies and magnetosome arrangements. This association suggests that inclusion formation is strain-dependent, although strongly modulated by local redox and nutrient conditions. Temporal changes in both freshly collected and stored samples show that MTB consortia respond rapidly to changing microenvironmental conditions, probably reflecting coupled microbial cycling of phosphorus, sulfur and carbonate in the sediment-water system. The dominance of large polyP-bearing cells in several microcosms further indicates that MTB may contribute to phosphorus sequestration even in small freshwater spring environments. These observations make the Kinizsi-spring assemblage a useful natural model for studying the ecological and geochemical roles of non-magnetic inclusions in MTB.

Acknowledgements

This research was funded by the National Research, Development and Innovation Office under programs RRF-2.3.1-21-2022-00014 and ADVANCED 152627. For the 3D reconstruction of morphologies the Dragonfly 3D world program (Version 2025.1) by Comet Technologies Canada Inc. was used (https://dragonfly.comet.tech/). We gratefully thank Dr. Éva Makó for the XRPD measurement.

References – Irodalom

Bazylinski, D. A. & Frankel, R. B. 2004: Magnetosome formation in prokaryotes. – *Nature Reviews Microbiology* **2**, 217–230. https://doi.org/10.1038/nrmicro842

Benzerara, K., Skouri-Panet, F., Li, J., Férard, C., Gugger, M., Laurent, T., Couradeau, E., Ragon, M., Cosmidis, J., Menguy, N., Margaret-Oliver, I., Tavera, R., López-García, P. & Moreira, D. 2014: Intracellular Ca-carbonate biomineralization is widespread in cyanobacteria. – *Proceedings of the National Academy of Sciences* **111**, 10933–10938. https://doi.org/10.1073/pnas.1403510111

Bidaud, C. C., Monteil, C. L., Menguy, N., Busigny, V., Jézéquel, D., Viollier, É., Travert, C., Skouri-Panet, F., Benzerara, K., Lefèvre, C. T. & Duprat, É. 2022: Biogeochemical niche of magnetotactic cocci capable of sequestering large polyphosphate inclusions in the anoxic layer of the Lake Pavin water column. – *Frontiers in Microbiology* **12**, 789134. https://doi.org/10.3389/fmicb.2021.789134

Blakemore, R. 1975: Magnetotactic bacteria. – *Science* **190**, 377–379. https://doi.org/10.1126/science.170679

Christ, J. J., Willbold, S. & Blank, L. M. 2020: Methods for the analysis of polyphosphate in the life sciences. – *Analytical Chemistry* **92**, 4167–4176. https://doi.org/10.1021/acs.analchem.9b05144

Couradeau, E., Benzerara, K., Gérard, E., Moreira, D., Bernard, S., Brown, G. E. & López-García, P. 2012: An early-branching microbialite cyanobacterium forms intracellular carbonates. – *Science* **336**, 459–462. https://doi.org/10.1126/science.1216171

Dahl, J.-U., Xie, L. & Jakob, U. 2018: Extraction and quantification of polyphosphate (polyP) from Gram-negative bacteria. – *Bio-protocol* **8,** e3011. https://doi.org/10.21769/bioprotoc.3011

Denoncourt, A. & Downey, M. 2021: Model systems for studying polyphosphate biology: a focus on microorganisms. – *Current Genetics* **67**, 331–346. https://doi.org/10.1007/s00294-020-01148-x

Devouard, B., Pósfai, M., Hua, X., Bazylinski, D. A., Frankel, R. B. & Buseck, P. R. 1998: Magnetite from magnetotactic bacteria; size distributions and twinning. – *American Mineralogist* **83**, 1387–1398. https://doi.org/10.2138/am-1998-11-1228

Diaz, J., Ingall, E., Benitez-Nelson, C., Paterson, D., de Jonge, M. D., McNulty, I. & Brandes, J. A. 2008: Marine polyphosphate: a key player in geologic phosphorus sequestration. – *Science* **320**, 652– 655. https://doi.org/10.1126/science.1151751

Faivre, D. & Schüler, D. 2008: Magnetotactic bacteria and magnetosomes. – *Chemical Reviews* **108**, 4875–4898. https://doi.org/10.1021/cr078258w

Flies, C. B., Peplies, J. & Schüler, D. 2005: Combined approach for characterization of uncultivated magnetotactic bacteria from various aquatic environments. – *Applied and Environmental Microbiology* **71**, 2723–2731. https://doi.org/10.1128/AEM.71.5.2723-2731.2005

Frankel, R. B., Blakemore, R. P. & Wolfe, R. S. 1979: Magnetite in freshwater magnetotactic bacteria. – *Science* **203**, 1355–1356. https://doi.org/10.1126/science.203.4387.1355

Frankel, R. B., Bazylinski, D. A., Johnson, M. S. & Taylor, B. L. 1997: Magneto-aerotaxis in marine coccoid bacteria. – *Biophysical Journal* **73**, 994–1000. https://doi.org/10.1016/s0006-3495(97)78132-3

Fuller, R. C. 1999: Microbial inclusions with special reference to PHA inclusions and intracellular boundary envelopes. – *International Journal of Biological Macromolecules* **25**, 2–29. https://doi.org/10.1016/s0141-8130(99)00011-2

Geohidroterv Kft. 2017: Nagyvázsony, 0328 hrsz-ú területen lévő egykori illegális hulladéklerakó: Részleges környezetvédelmi felülvizsgálat és rekultivációs terv [Partial environmental review and remediation plan for the former illegal waste disposal site at property no. 0328, Nagyvázsony] (Report No. G-2017/12)

Goswami, P., He, K., Li, J., Pan, Y., Roberts, A. P. & Lin, W. 2022: Magnetotactic bacteria and magnetofossils: ecology, evolution and environmental implications. – *Biofilms and Microbiomes* **8,** 43. https://doi.org/10.1038/s41522-022-00304-0

Hupfer, M., Gloess, S. & Grossart, H.-P. 2007: Polyphosphate-accumulating microorganisms in aquatic sediments. – *Aquatic Microbial Ecology* **47,** 299–311. https://doi.org/10.3354/ame047299

Kasama, T., Pósfai, M., Chong, R. K. K., Finlayson, A. P., Buseck, P. R., Frankel, R. B. & Dunin-Borkowski, R. E. 2006: Magnetic properties, microstructure, composition, and morphology of greigite nanocrystals in magnetotactic bacteria from electron holography and tomography. – *American Mineralogist* **91**, 1216–1229. https://doi.org/10.2138/am.2006.2227

Keim, C. N., Solórzano, G., Farina, M. & Lins, U. 2005: Intracellular inclusions of uncultured magnetotactic bacteria. – *International Microbiology* **8**, 111–117.

Kim, K.-S., Rao, N. N., Fraley, C. D. & Kornberg, A. 2002: Inorganic polyphosphate is essential for long-term survival and virulence factors in *Shigella* and *Salmonella* spp. – *Proceedings of the National Academy of Sciences* **99**, 7675–7680. https://doi.org/10.1073/pnas.112210499

Kósa I. & Pósfai M. 2007: Mágneses baktériumok a Balatonban. – *Hidrológiai Közlöny* **87**, 90–92.

Lefèvre, C. T., Pósfai, M., Abreu, F., Lins, U., Frankel, R. B. & Bazylinski, D. A. 2011: Morphological features of elongated-anisotropic

magnetosome crystals in magnetotactic bacteria of the Nitrospirae phylum and the Deltaproteobacteria class. – *Earth and Planetary Science Letters* **312**, 194–200. https://doi.org/10.1016/j.epsl.2011.10.003

LI, J., MENGUY, N., GATEL, C., BOUREAU, V., SNOECK, E., PATRIARCHE, G., LEROY, E. & PAN, Y. 2015: Crystal growth of bullet-shaped magnetite in magnetotactic bacteria of the Nitrospirae phylum. – *Journal of The Royal Society Interface* **12**, 20141288. https://doi.org/10.1098/rsif.2014.1288

LI, J., MENGUY, N., ROBERTS, A. P., GU, L., LEROY, E., BOURGON, J., YANG, X., ZHAO, X., LIU, P., CHANGELA, H. G. & PAN, Y. 2020: Bullet shaped magnetite biomineralization within a magnetotactic Deltaproteobacterium: implications for magnetofossil identification. – *Journal of Geophysical Research: Biogeosciences* **125**, e2020JG005680. https://doi.org/10.1029/2020jg005680

LI, J., LIU, P., TAMAXIA, A., ZHANG, H., LIU, Y., WANG, J., MENGUY, N., ZHAO, X., ROBERTS, A. P. & PAN, Y. 2021: Diverse intracellular inclusion types within magnetotactic bacteria: implications for biogeochemical cycling in aquatic environments. – *Journal of Geophysical Research: Biogeosciences* **126**, e2021JG006310. https://doi.org/10.1029/2021JG006310

LIU, P., LIU, Y., ZHAO, X., ROBERTS, A. P., ZHANG, H., ZHENG, Y., WANG, F., WANG, L., MENGUY, N., PAN, Y. & LI, J. 2021: Diverse phylogeny and morphology of magnetite biomineralized by magnetotactic cocci. – *Environmental Microbiology* **23**, 1115–1129. https://doi.org/10.1111/1462-2920.15254

LIU, P., ZHENG, Y., ZHANG, R., BAI, J., ZHU, K., BENZERARA, K., MENGUY, N., ZHAO, X., ROBERTS, A. P., PAN, Y. & LI, J. 2023: Key gene networks that control magnetosome biomineralization in magnetotactic bacteria. – *National Science Review* **10**, nwac238. https://doi.org/10.1093/nsr/nwac238

LIU, P., ZHANG, R., MENG, F., ZHANG, C., ROBERTS, A. P., WANG, Y., ZHU, K., CAO, Z., PAN, Y. & LI, J. 2025: Deep-branching magnetotactic bacteria form intracellular carbonates enriched in trace metals. – *mSystems* **10**, e01131- 25. https://doi.org/10.1128/msystems.01131-25

MANGIN, C. C., BENZERARA, K., BERGOT, M., MENGUY, N., ALONSO, B., FOUTEAU, S., MÉHEUST, R., CHEVRIER, D. M., GODON, C., TURRINI, E., MEHTA, N., DUVERGER, A., TRAVERT, C., BUSIGNY, V., DUPRAT, E., BOLZONI, R., CRUAUD, C., VIOLLIER, E., JÉZÉQUEL, D., VALLENET, D., LEFÈVRE, C. T. & MONTEIL, C. L. 2025: Magnetotactic bacteria affiliated with diverse Pseudomonadota families biomineralize intracellular Ca-carbonate. – *The ISME Journal: Multidisciplinary Journal of Microbial Ecology* **19**, wrae260. https://doi.org/10.1093/ismejo/wrae260

MANN, S., SPARKS, N. H. C., FRANKEL, R. B., BAZYLINSKI, D. A. & JANNASCH, H. W. 1990: Biomineralization of ferrimagnetic greigite (Fe_3S_4) and iron pyrite (FeS_2) in a magnetotactic bacterium. – *Nature* **343**, 258–261. https://doi.org/10.1038/343258a0

MASON-JONES, K., ROBINSON, S. L., VEEN, G. F., MANZONI, S. & VAN DER PUTTEN, W. H. 2022: Microbial storage and its implications for soil ecology. – *The ISME Journal: Multidisciplinary Journal of Microbial Ecology* **16**, 617–629. https://doi.org/10.1038/s41396-021-01110-w

MONTEIL, C. L., BENZERARA, K., MENGUY, N., BIDAUD, C. C., MICHOT-ACHDJIAN, E., BOLZONI, R., MATHON, F. P., COUTAUD, M., ALONSO, B., GARAU, C., JÉZÉQUEL, D., VIOLLIER, E., GINET, N., FLORIANI, M., SWARAJ, S., SACHSE, M., BUSIGNY, V., DUPRAT, E., GUYOT, F. & LEFÈVRE, C. T. 2021: Intracellular amorphous Ca-carbonate and magnetite biomineralization by a magnetotactic bacterium affiliated to the Alphaproteobacteria. – *The ISME Journal: Multidisciplinary Journal of Microbial Ecology* **15**, 1–18. https://doi.org/10.1038/s41396-020-00747-3

PÓSFAI, M., BUSECK, P. R., BAZYLINSKI, D. A. & FRANKEL, R. B. 1998: Iron sulfides from magnetotactic bacteria; structure, composition, and phase transitions. – *American Mineralogist* **83**, 1469–1481. https://doi.org/10.2138/am-1998-11-1235

PÓSFAI, M. & ARATÓ, B. 2000: Magnetotactic bacteria and their mineral inclusions from Hungarian freshwater sediments. – *Acta Geologica Hungarica* **43**, 463–476.

PÓSFAI, M., LEFÈVRE, C. T., TRUBITSYN, D., BAZYLINSKI, D. A. & FRANKEL, R. B. 2013: Phylogenetic significance of composition and crystal morphology of magnetosome minerals. – *Frontiers in Microbiology* **4/344**. https://doi.org/10.3389/fmicb.2013.00344

POWELL, N., SHILTON, A., CHRISTI, Y. & PRATT, S. 2009: Towards a luxury uptake process via microalgae – defining the polyphosphate dynamics. – *Water Research* **43**, 4207–4213. https://doi.org/10.1016/j.watres.2009.06.011

RÁCZ, K., NYIRŐ-KÓSA, I., KÖVÉR, R., MOLNÁR, ZS., SOMOGYI, B., KOVÁCS W., A., ISTVÁNOVICS, V. & PÓSFAI, M. 2026: Biogenic origin and clay-assisted sink of 'visible phosphorus' in a shallow, calcareous lake. – *Biogeochemistry* **169/40**. https://doi.org/10.1007/s10533-026-01329-9

RIVAS-LAMELO, S., BENZERARA, K., LEFÈVRE, C. T., MONTEIL, C.L., JÉZÉQUEL, D., MENGUY, N., VIOLLIER, E., GUYOT, F., FÉRARD, C., POINSOT, M., SKOURI-PANET, F., TRCERA, N., MIOT, J. & DUPRAT, E. 2017: Magnetotactic bacteria as a new model for P sequestration in the ferruginous Lake Pavin. – *Geochemical Perspectives Letters* **5**, 35–41. https://doi.org/10.7185/geochemlet.1743

SCHULZ-VOGT, H. N., POLLEHNE, F., JÜRGENS, K., ARZ, H. W., BEIER, S., BAHLO, R., DELLWIG, O., HENKEL, J. V., HERLEMANN, D. P. R., KRÜGER, S., LEIPE, T. & SCHOTT, T. 2019: Effect of large magnetotactic bacteria with polyphosphate inclusions on the phosphate profile of the suboxic zone in the Black Sea. – *The ISME Journal: Multidisciplinary Journal of Microbial Ecology* **13**, 1198–1208. https://doi.org/10.1038/s41396-018-0315-6

SEKERCI, F., FISCHER, S., JOSHI, P., PEIFFER, S., KAPPLER, A. & MANSOR, M. 2025: Sulfur microenvironments as hotspots for biogenic pyrite formation. – *Scientific Reports* **15,** 20148. https://doi.org/10.1038/s41598-025-05178-8

SHIMOSHIGE, H., YANAGISAWA, K., MIYAZAKI, M., TAKAKI, Y., SHIMAMURA, S., NOMAKI, H., FUKUI, M., SHIRAKAWA, H., KOBAYASHI, H., TAOKA, A. & MAEKAWA, T. 2025: Isolation and cultivation of a novel freshwater magnetotactic coccus FCR-1 containing unchained magnetosomes. – *Communications Biology* **8**, 505. https://doi.org/10.1038/s42003-025-07981-5

TÓTH Á. Z. 2018: *A Balaton-felvidék felszínalatti vizeinek hidraulikai kapcsolata a Bakonnyal és a Balatonnal.* – PhD dissertation, Eötvös Loránd University, Budapest. https://doi.org/10.15476/ELTE.2018.123

WEYLAND, M., YATES, T. J. V., DUNIN-BORKOWSKI, R. E., LAFFONT, L. & MIDGLEY, P. A. 2006: Nanoscale analysis of three-dimensional structures by electron tomography. – *Scripta Materialia* **55**, 29–33. https://doi.org/10.1016/j.scriptamat.2005.12.058

Manuscript received: 2026/06/16

Supporting Information

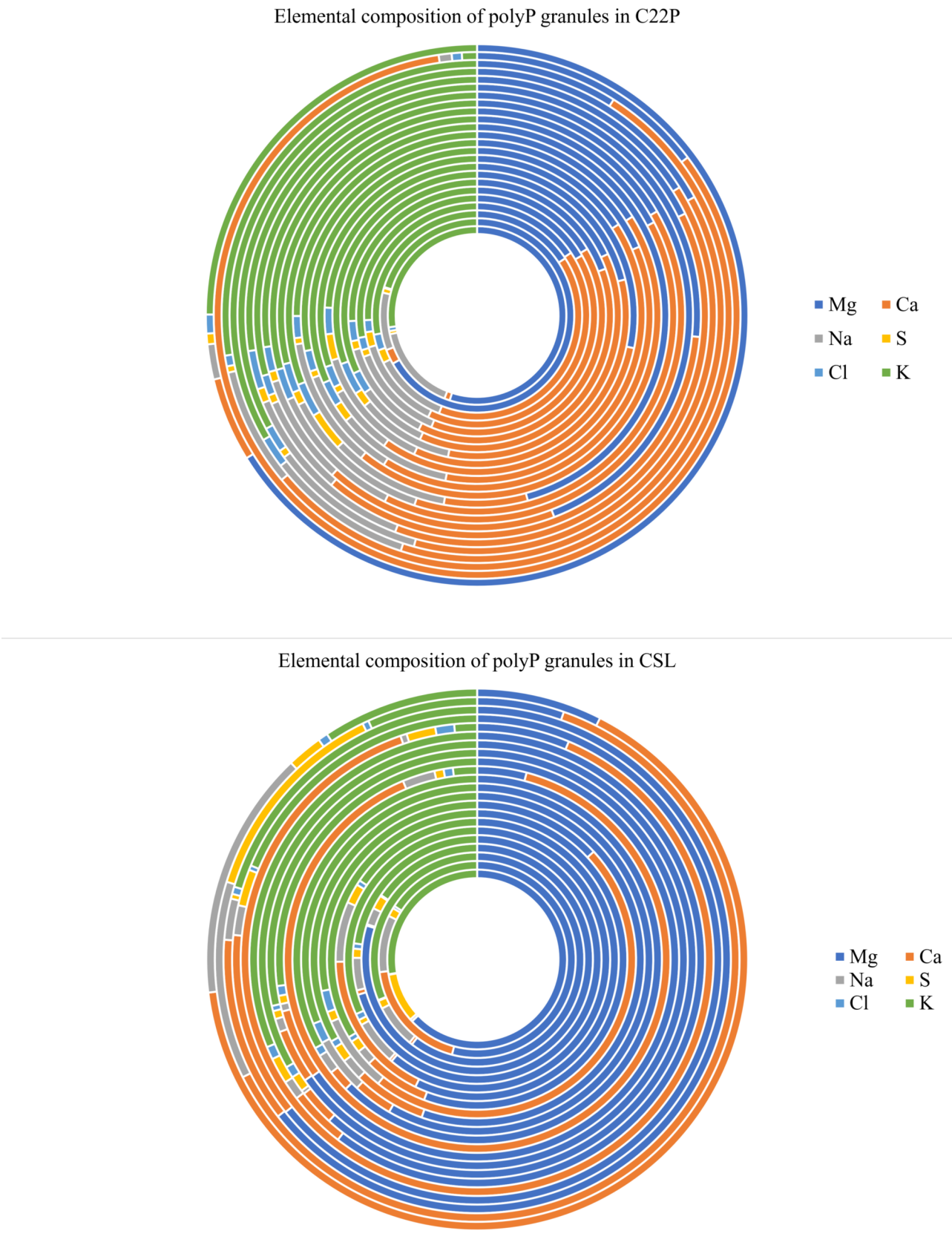


Figure S1. Elemental compositions of polyP granules in C2P and CSL cell types on a doughnut chart. Each individual circle in the chart corresponds to a cell. P and O elements are not plotted.

S1. ábra. *C2P és CSL sejtek polyP zárványainak elemi összetétele perecdiagrammon ábrázolva. Mindegyik kör egy adott sejtet jelöl. A P és O elemek nincsenek ábrázolva.*

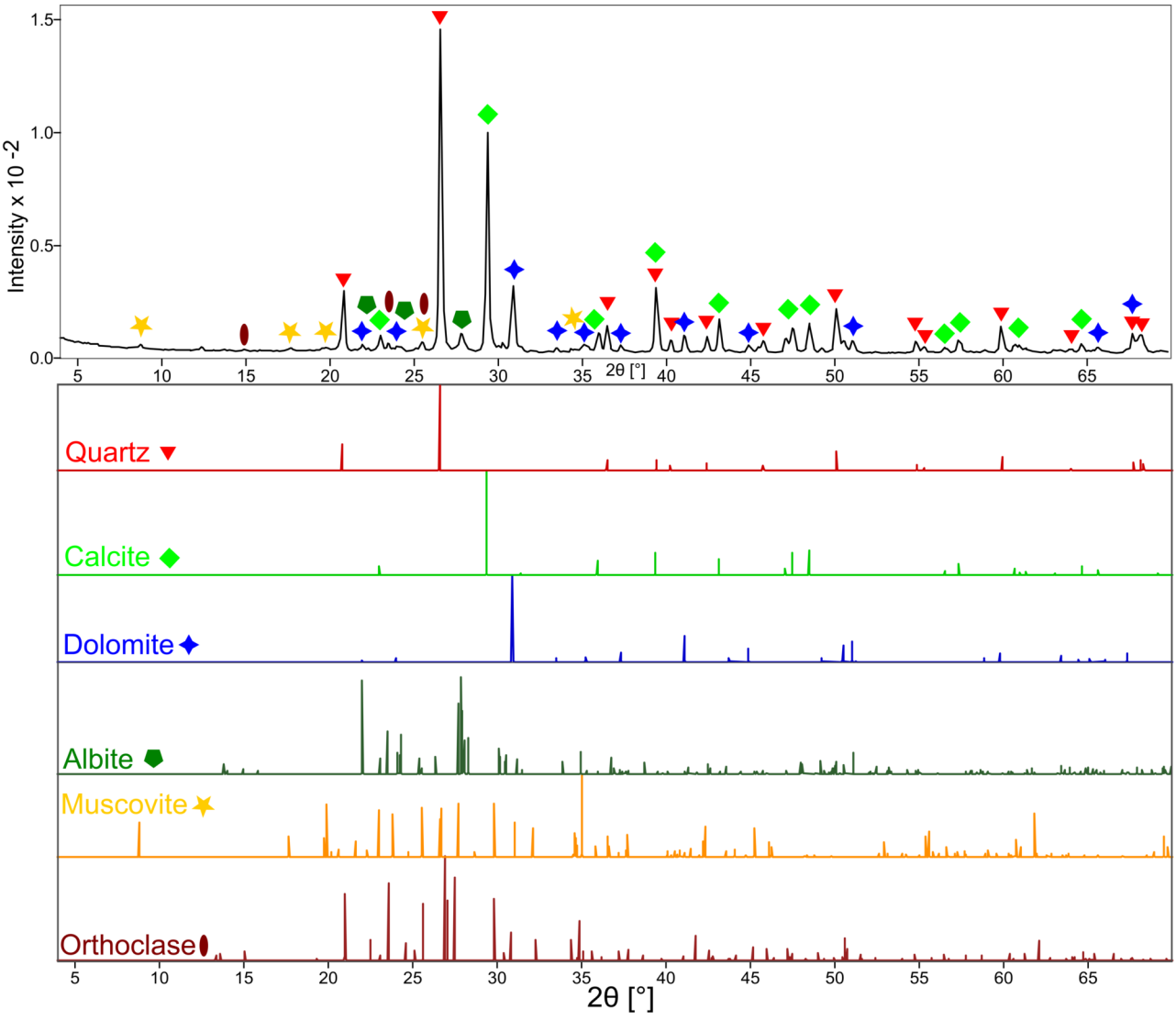


Figure S2. XRPD pattern of the sediment of the 'D' microcosm of the sample collected in January 2025. The sample consists predominantly of quartz and carbonates (calcite and dolomite), and some silicates (albite, orthoclase and muscovite).

S2. ábra. *XRPD-mérés eredménye a 2025. januári 'D' mikrokozmosz üledékéről. A mintában uralkodóan kvarc és karbonátok (kalcit és dolomit), valamint szilikátok (albit, ortoklász, muszkovit) fordulnak elő.*

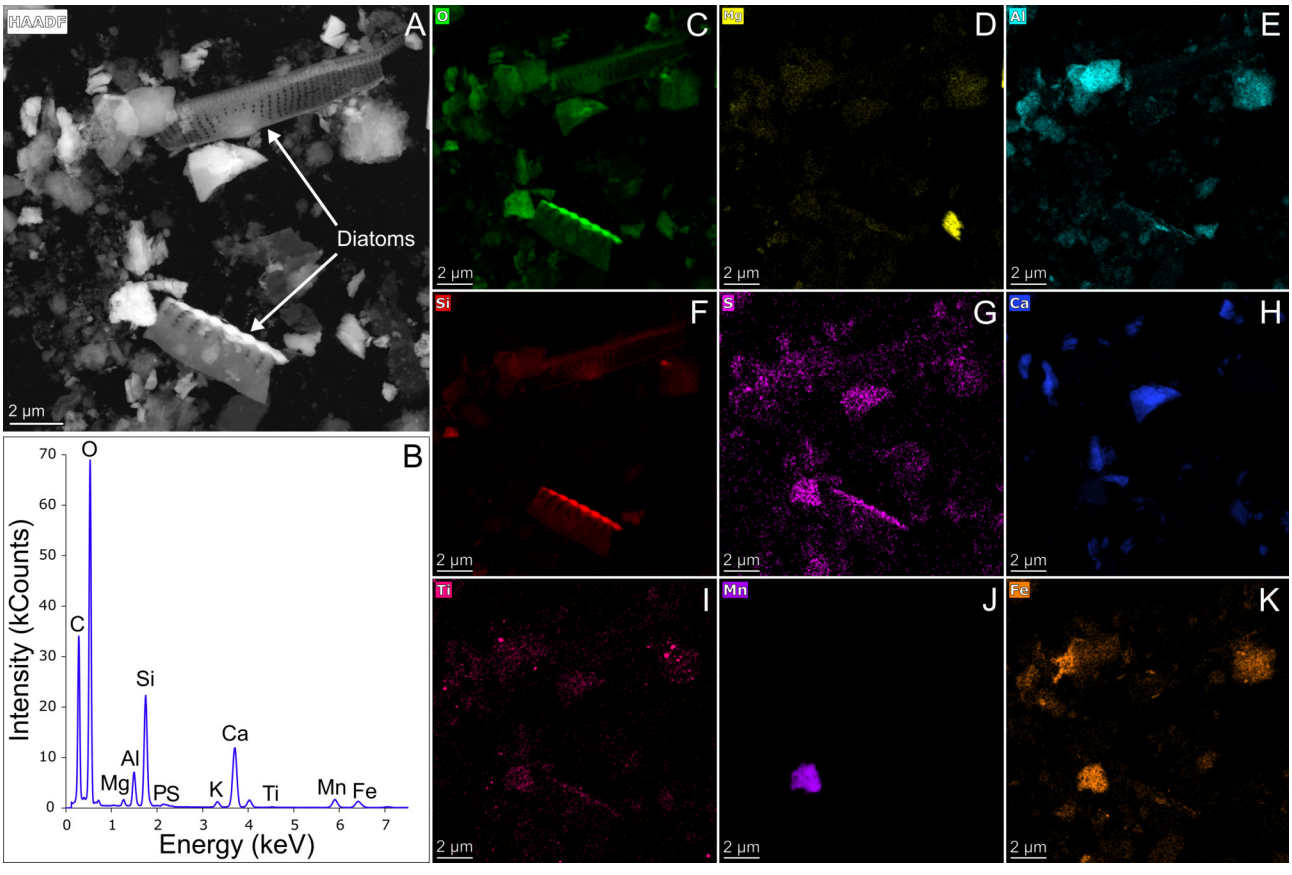


Figure S3. (A) A typical STEM HAADF image of the sediment in 'D' microcosm of the sample collected in January 2025, with (B) an EDS spectrum of the whole imaged area and (C-K) EDS elemental maps of the sediment. In addition to carbonate and silicate minerals, two diatom fragments (marked with white arrows) are also present.

S3. ábra. *(A) A 2025. januári 'D' mikrokozmosz üledékéről készített tipikus STEM HAADF-felvétel, (B) a kép teljes területéről összegzett EDS-spektrummal és (C-K) EDS-elemtérképekkel. A karbonát- és szilikátásványok mellett két kovaalga-töredék (fehér nyilakkal jelölve) is látható.*